Water Research 155 (2019) 66–75

Contents lists available at ScienceDirect

Water Research

journal homepage: www.elsevier.com/locate/watres

Micro-milling super-fine powdered activated carbon decreases adsorption capacity by introducing oxygen/hydrogen-containing functional groups on carbon surface from water

Hideki Takaesu [a], Yoshihiko Matsui [b, *], Yuki Nishimura [a], Taku Matsushita [b], Nobutaka Shirasaki [b]

[a] Graduate School of Engineering, Hokkaido University, Japan
[b] Faculty of Engineering, Hokkaido University, Japan

ARTICLE INFO

Article history:
Received 4 December 2018
Received in revised form
4 February 2019
Accepted 6 February 2019
Available online 20 February 2019

Keywords:
SPAC
Geosmin
Bentazone
Isotherm
Mechanochemical reaction

ABSTRACT

Superfine powdered activated carbon (SPAC) of micron to submicron particle size is produced by micro-milling of conventionally sized powdered activated carbon. SPAC has attracted attention because of its high adsorption capacity; however, milling to the submicron particle size range lowers its adsorption capacity. Here, we found that this decrease of adsorption capacity was due to the introduction of oxygen/hydrogen-containing functional groups into the graphene structure of the carbon from water during the milling, causing it to become less hydrophobic. This finding was supported by three analyses of SPAC particles before and after milling: 1) elemental analysis revealed increased oxygen and hydrogen content, 2) Boehm titration analysis revealed increased amounts of acidic functional groups, including carboxylic and phenolic hydroxyl groups, and 3) Fourier-transform infrared spectroscopy showed increased peaks at 1200, 1580, and 3400 cm^{-1}, confirming the presence of those groups. Dissolved oxygen concentration did not strongly affect the increase of oxygen content in SPAC, and no evidence was found for hydroxyl radical production during micro-milling, suggesting that a mechanochemical reaction underlies the increase in oxygen/hydrogen-containing functional groups. An increase in ^{18}O content in the SPAC particles after milling in water-^{18}O indicated that the oxygen in the functional groups originated from the surrounding water.

1. Introduction

Superfine powdered activated carbon (SPAC) has attracted attention for its high adsorption capacity and kinetics (Amaral et al., 2016; Ando et al., 2010; Bonvin et al., 2016; Dunn and Knappe, 2013; Heijman et al., 2009; Jiang et al., 2015; Matsui et al. 2004, 2012, 2015). In full-scale water treatment plants, SPAC with a particle diameter of 1–3 μm, produced onsite from conventional-size powdered activated carbon (PAC), is currently used as an adsorbent during pretreatment before membrane filtration (Kanaya et al., 2015). Micro-milling technology is now able to produce submicron SPAC (SSPAC) with a particle diameter down to 140 nm (Ellerie et al., 2013; Pan et al., 2017a; Partlan et al., 2016). However, it has been shown that micro-milling increases the oxygen content of activated carbon (AC) (Partlan et al., 2016) and decreases its capacity to adsorb 2-methylisoborneol (MIB) (Pan et al., 2017a), although the internal pore volume and surface area of AC particles are not substantially changed (Pan et al., 2017b; Partlan et al., 2016). Similarly, it has also been reported that ball-milling has no effect on the structure of AC particles (Welham and Williams, 1998).

AC with a low oxygen content has a greater capacity than AC with a high oxygen content for adsorption of hydrophobic micro-pollutants such as MIB (Considine et al., 2001; Pendleton et al., 1997). Oxygen can form various oxygen-containing functional groups, such as carboxyl, carbonyl and phenolic hydroxyl functional groups, on the AC particle surface, which promote the formation of water clusters at the particle surface that impede, or prevent, the adsorption of hydrophobic micro-pollutants (Pendleton et al., 2002; Quinlivan et al., 2005).

Thus, it can be hypothesized that micro-milling promotes the formation of oxygen-containing functional groups at the AC particle surface, causing the oxygen content of the AC to increase and its

* Corresponding author. North13, West 8, Sapporo, 060-8628, Japan.
E-mail address: matsui@eng.hokudai.ac.jp (Y. Matsui).

https://doi.org/10.1016/j.watres.2019.02.019
0043-1354/

adsorption capacity to decrease; this hypothesis, and the underlying mechanism, have yet to be confirmed, although the underlying mechanism may involve a mechanochemical reaction (Balaz et al., 2013). Micro-milling AC particles and the changes of the characteristics of AC particles induced by micro-milling are important issues for optimizing SPAC for the efficient removal of micro-pollutants from water (Partlan et al., 2016).

Here, we clarified that the amount of oxygen/hydrogen-containing functional groups on the surface of AC particles is increased by micro-milling and investigated the causes of this increase. Three environmentally relevant micro-pollutants were selected as target adsorbates (WHO, 2011): MIB, geosmin, and bentazone. MIB and geosmin are cyanobacterial metabolites that influence the quality of drinking water due to their strong, earthy or musty taste and odor with a very low odor detection threshold. These compounds can be removed from water by adsorption onto AC because of their hydrophobicity (log Kow value, 3.31 and 3.57, respectively), although the amount removed is variable. Bentazone is a pesticide that because of its high hydrophilicity (log Kow value, −0.46) is not readily adsorbed by AC.

2. Experimental

2.1. Activated carbons

Three wood-based PACs (W-TK, W-TKO and W-SR) and two coconut-based PACs (C-TK and C-SR) with median diameters (D50s) of 4–24 μm were obtained from Futamura Chemical Co., Tokyo, Japan (W-TK, W-TKO and C-TK) and Osaka Chemical Co., Osaka, Japan (W-SR and C-SR). Large SPAC ($SPAC_L$; D50, 2.3–5.1 μm) was produced by wet-milling these PACs with a ball mill (Nikkato, Osaka, Japan). Small SPAC ($SPAC_S$, 0.9–1.4 μm) and SSPAC (0.13–0.23 μm) were produced with a bead mill (LMZ015, Ashizawa Finetech, Chiba, Japan). Details of the milling procedures are as follows.

Normal milling procedure: $SPAC_L$ was obtained by ball-milling PACs slurry (15% w/w) at 45 rpm for 4–5 h. After diluting the $SPAC_L$ slurry with pure water to approximately 1% (w/w), the $SPAC_L$ was bead-milled with ZrO_2 beads (ϕ 0.3 mm) at a speed of 8 m/s (2590 rpm) for 20–30 min and $SPAC_S$ was obtained. SSPAC were obtained by bead-milling $SPAC_L$ using ZrO_2 beads (ϕ 0.1 mm) at 12 m/s (3884 rpm) unless otherwise specified for 1.5–6 h. A cooling system kept the temperature of the slurry below 28 °C during bead-milling.

Anoxic milling procedure: After drying PAC in a vacuum chamber for >1 h, the PAC was rinsed with pure water three times in a glove box filled with nitrogen gas. After preparing the PAC slurry of 15% (w/w), the PAC slurry was transferred to the ball mill in the glove box. $SPAC_L$ slurry was obtained by ball-milling the PAC slurry. The $SPAC_L$ slurry concentration was adjusted to about 1% (w/w), and then the DO of the slurry was removed to < 1 mg/L by purging with nitrogen gas. $SPAC_S$ and SSPAC were obtained by bead milling the $SPAC_L$ slurry under nitrogen gas purging. The other conditions of the anoxic milling were the same as those of the normal milling.

2.2. AC characterization

2.2.1. Particle size

AC slurries (50 mL) were supplemented with dispersant (0.08% w/v, Triton X-100, Kanto Chemical, Tokyo, Japan), and then they were ultra-sonicated (150 W, 19.5 kHz) for 6 min (SSPAC) or 1 min (PAC, $SPAC_L$ and $SPAC_S$). Particle sizes of the ACs were determined by a Microtrac analyzer (MT3300EXII, Nikkiso, Tokyo, Japan) (Pan et al., 2017a).

2.2.2. Elemental analysis

Elemental compositions (H, C, N, O and S) of ACs were determined according to the procedure of Pan et al. (2017a). In brief, after drying AC slurries under vacuum at ~20 °C, the ACs were packed in silver capsules, and then the capsules were weighed. After the capsules were placed under vacuum, they were transferred to a CHNS/O elemental analyzer (Vario EL Cube, Elementar Japan, Yokohama, Japan) to measure the elemental contents. Triplicate measurements were conducted for each AC sample to give the average.

2.2.3. Boehm titration method

Boehm titration (Biniak et al., 1997; Noh and Schwarz, 1990) was applied to determine the surface functional groups of the ACs. AC slurry containing 200 mg of AC in a glass test tube was supplemented with 0.1 N NaOH, Na_2CO_3, $NaHCO_3$, or HCl solution of the same volume as the AC slurry. The resulting slurry was placed under a vacuum and then under a N_2 atmosphere. After sealing the tube containing the slurry, the tube was shaken at 20 °C for 2 days. After centrifugation (4000 rpm, 2764*g*) of the slurry, the supernatant was filtered through a hydrophilic polytetrafluoroethylene membrane (0.2-μm pore size, Toyo Roshi Kaisha, Tokyo, Japan). The filtrate (10 mL) was mixed with a HCl (0.05 N, 20 mL) or NaOH (0.05 N, 20 mL) solution. After the mixture was sparged with N_2 gas for 45–60 min, it was back-titrated with a NaOH or HCl solution to quantify the uptake of one of the bases (NaOH or Na_2CO_3, $NaHCO_3$) or the acid (HCl). By assuming that $NaHCO_3$ neutralized carboxylic groups only, Na_2CO_3 neutralized carboxylic and lactonic groups, and NaOH neutralized all acidic groups including the phenolic hydroxyl group (Boehm 1966, 2002), the differences between the uptakes of the bases was used to estimate the amount of sites with one specific acid group (carboxylic, lactonic, or phenolic hydroxyl group). The amount of basic sites was calculated from the amount of HCl required in the titration. All chemicals used were reagent grade (Wako Pure Chemical Industries, Osaka, Japan).

2.2.4. Fourier-transform infrared spectroscopy

AC slurries were dried under vacuum at ~20 °C to avoid oxidation during drying. The dried samples were mixed with KBr at 1:500 mass ratio. The mixture was compacted into a pellet, and the pellet was kept under vacuum before transmission measurement. The transmission measurement was conducted with a Fourier-transform infrared spectroscopy (FTIR) spectrometer (FTIR-8400S, Shimadzu, Kyoto, Japan).

2.2.5. Production of SSPAC in water-^{18}O and isotope analysis

After rinsing with pure water three times, the slurry of PAC was ball-milled by the normal milling procedure to produce $SPAC_L$ slurry. $SPAC_L$ slurry (500 mL) was supplemented with 3 mL of ^{18}O-enriched water (10 at.%, Taiyo Nippon Sanso, Tokyo, Japan). The supplemented slurry was then bead-milled under the anoxic condition for 2–6 h at 12 m/s with ϕ 0.1-mm beads to produce SSPAC. The AC slurries were dried under vacuum at ~20 °C and then capsuled for isotope ratio analysis. Capsulation in a glovebox filled with nitrogen gas was also conducted. Isotope ratio analysis was conducted to determine the isotopic composition of the samples by using an ANCA-GSL elemental analyzer (Sercon, Cheshire, UK) in the analytical laboratory (Kyoto, Japan) of Taiyo Nippon Sanso. $\delta^{18}O$ values were calculated from the $^{18}O/^{16}O$ ratios.

A control experiment was conducted in which a portion (10 mL) of SSPAC produced by 2- or 6-h bead-milling under the anoxic condition was supplemented with 0.056 mL of ^{18}O-enriched water (10 at.%) and mixed with no milling for 2–6 h. The AC slurry was then dried under vacuum at ~20 °C and capsuled for isotope ratio analysis.

2.3. Adsorption experiments

The working solutions of MIB, geosmin, and bentazone were prepared by adding each reagent-grade chemical (Wako Pure Chemical Industries) to organic-free ionic water: the ion composition was the same as those used in previous researches (Matsui et al., 2015; Pan et al., 2016). Batch adsorption isotherm tests were conducted by the bottle-point technique (Pan et al., 2017a). Different amounts of AC were added to 110-mL vials containing the working solutions. Immediately after the AC addition, the vials were shaken on a rotary shaker at 20 °C in the dark (Matsui et al. 2012, 2013). After shaking for 1 week for PAC and $SPAC_L$ or 3 days for $SPAC_S$ and SSPAC, the AC particles were separated by filtering the solution through a hydrophilic polytetrafluoroethylene membrane, and the liquid-phase adsorbate concentrations were measured. Adsorbate concentrations in solid phase were calculated from mass balances.

MIB concentrations were determined by purge and trap gas chromatography/mass spectrometry (Aqua PT 5000 J, GL Sciences, Tokyo, Japan; GCMS-QP2010 Plus, Shimadzu, Kyoto, Japan) or headspace–solid-phase microextraction gas chromatography/mass spectrometry (PAL RSI 85; 7820A/5977 E MSD, Agilent Agilent Technologies Japan) according to the procedure of Pan et al. (2017a). Geosmin concentration was determined by methods similar to those used for MIB. The bentazone concentration was determined by liquid chromatography/Orbitrap mass spectrometry (Q Exactive; UltiMate3000 LC systems, Thermo Fisher Scientific, Tokyo, Japan) using a Hypersil GOLD column (1.9 μm, 50 mm × 2.1 mm), a temperature of 40 °C, a mobile phase (methanol:2 mM formic acid = 70:30), and flow rate of 0.2 mL/min; *m/z* 239.0496 was attributed to bentazone.

3. Results and discussion

3.1. Adsorption capacity

Adsorption isotherms of MIB, geosmin, and bentazone on the wood-based and coconut-based ACs of different particle sizes were obtained to observe how adsorption capacity was changed by milling. The adsorption isotherms were changed with milling. Changes of isotherms with particle size are depicted in Figs. 1S–4S. Because the slopes in the plot of log-*q* vs. log-*c* plot were almost the same, where *q* and *c* denote solid-phase and liquid-phase concentrations, respectively, the adsorption capacity of each AC for each adsorbate was then represented by the solid-phase concentration at a specific liquid-phase concentration, after describing the isotherm data by the Freundlich equation.

For MIB adsorption on the various ACs, we confirmed the trend reported by Pan et al. (2017a), who observed that the MIB adsorption capacity of a wood-based AC increased with decreasing particle diameter from 10 to 1 μm, but decreased with decreasing particle diameter from 1 to 0.2 μm (Fig. 1). In the present study, the changes in adsorption capacity for geosmin were more prominent than those for MIB. In addition to the changes observed for the hydrophobic compounds MIB and geosmin, a similar trend was observed for the highly hydrophilic compound bentazone. Pan et al. (2017a) attributed the decrease of adsorption capacity with decreasing particle size in the submicron-diameter range to the AC oxidation during micro-milling, and the increase of adsorption capacity in the 10-μm diameter range to adsorption on the external particle surface, and they presented a correlation between adsorption capacity and oxygen content of AC particles with diameters less than 2 μm ($SPAC_S$ and SSPAC). For such small-size AC, adsorption occurs both internally and externally, suggesting that pore surface chemistry, as represented by oxygen content, strongly affects adsorption capacity. To assess the adsorption of geosmin, bentazone, and MIB on the different ACs, we examined the correlations between adsorption capacities and oxygen content (Fig. 2) and verified that the reduction of adsorption capacity during micro-milling was related to the increase of the oxygen content of the AC particles.

3.2. Changes in the amounts of oxygen-containing functional groups and elemental composition

The results of the elemental analysis are shown in Fig. 3 and 5S. The oxygen content of the ACs increased with decreasing particle size, which is in accordance with the results of previous studies (Dunn and Knappe, 2013; Partlan et al., 2016). In our study, the diameter of AC particles did not change substantially after the median diameter reached around 150 nm. Thus, this diameter was considered to be the minimum critical median particle diameter (equilibrium state) of our micro-milling system. However, the oxygen content of the ACs continued to increase with increasing milling time, even after the equilibrium state had been reached. The equilibrium state of milling is related not only to aggregation/agglomeration, but also to fracture, of the AC particles (Balaz et al., 2013; Berndt, 2004). Thus, our data suggest that although particle size remained unchanged once the equilibrium state was reached, the AC particles were fractured, and new particle surfaces were generated with continued milling.

A similar trend was observed for hydrogen (Figs. 3 and 5S). The hydrogen content of the ACs increased with milling, although the total hydrogen content remained small. The increase in hydrogen content is briefly noted by Pan et al. (2017a), but the supporting data is limited. Our data clearly showed that the increase in hydrogen content was in proportion to the increase in oxygen content (Fig. 3, lower right panel, and Fig. 5S). In contrast, the carbon content of the ACs decreased, and the nitrogen and sulfate content remained small and unchanged.

According to our Boehm titration observations, the amount of acidic functional groups increased with increasing oxygen content during milling, whereas the amount of basic functional groups decreased (Fig. 6S). The decrease in the amount of basic groups was approximately half the increase in the amount of acidic groups; therefore, the total number of functional groups was increased. When acidic groups were differentiated by selective neutralization with bases of different basicities, the data indicated increases in the amounts of phenolic hydroxyl, lactonic, and carboxylic groups (Fig. 4). In addition, the rates of increase against oxygen content were similar for each acidic group regardless initial oxygen content and initial amounts of functional groups. Although W-TKO AC had higher oxygen content, higher amounts of phenolic hydroxyl and lactonic groups, and lower amount of carboxylic groups than W-TK and C-SR ACs, the rates of functional group increases against oxygen contents were similar. Therefore, reaction to introduce these functional groups might occur on the basic structure of AC.

The basic character of AC with a graphene structure free from oxygen is the result of basic sites arising from delocalized π-electrons as well as the presence of basic groups such as ketones, pyrones, chromenes, ethers, and carbonyls at the particle surface (Shafeeyan et al., 2010). Therefore, the decrease in the amount of basic functional groups was likely due to loss of these basic groups and the graphene structure.

FTIR spectrums of the ACs are shown in Fig. 5. As milling progressed, increases were observed for the peaks around 1200 cm^{-1}, which were assigned to C-O and C-OH; the peak around 3400 cm^{-1}, which was assigned to O-H (Barroso-Bogeat et al., 2014; Fanning and Vannice, 1993; Shafeeyan et al., 2010); and the peak around 1580 cm^{-1}, which was ascribed to the presence of vicinal hydroxyl

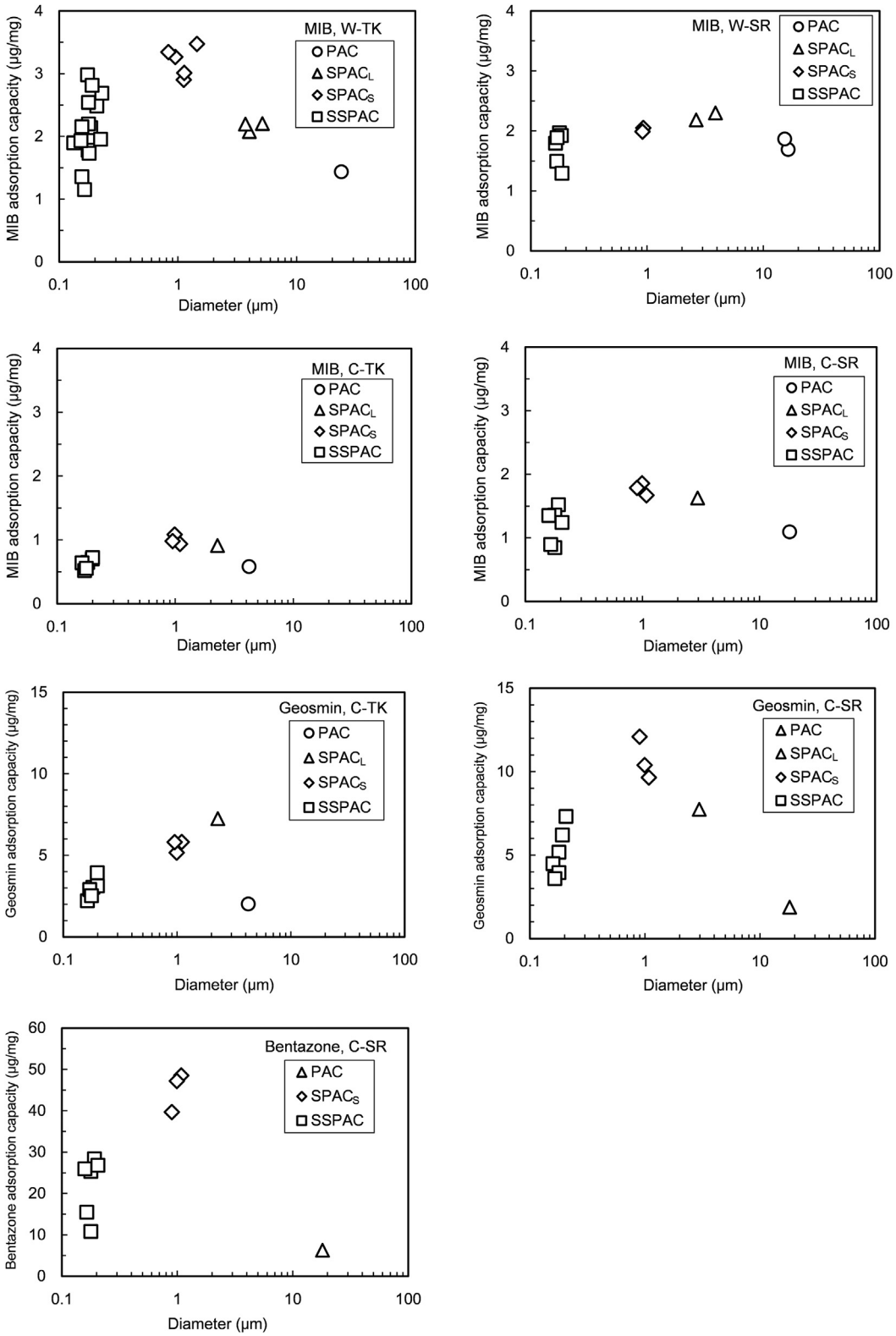

Fig. 1. Change of adsorption capacity with AC particle size. The values on the y-axis were quantified in terms of the solid-phase concentration for an equilibrium liquid-phase concentration of 50 ng/L for MIB and geosmin and 5 μg/L for bentazone (see also Figs. 1S–4S).

groups (Fuente et al., 2003) (Note: while the increase of the peak 3400 cm^{-1} was distinct for W-TK and C-SR ACs, the increase was faint for W-TKO AC. The reason was not clearly understood). Overall, both the Boehm and FTIR data indicate the formation of carboxylic and phenolic hydroxyl groups. The peak around 1700 cm^{-1}, which was assigned to C=O in acidic (carboxylic and lactonic) and basic groups (ketone, pyrone, etc.), was unchanged. The increase in the amount of acidic groups and the decrease in the

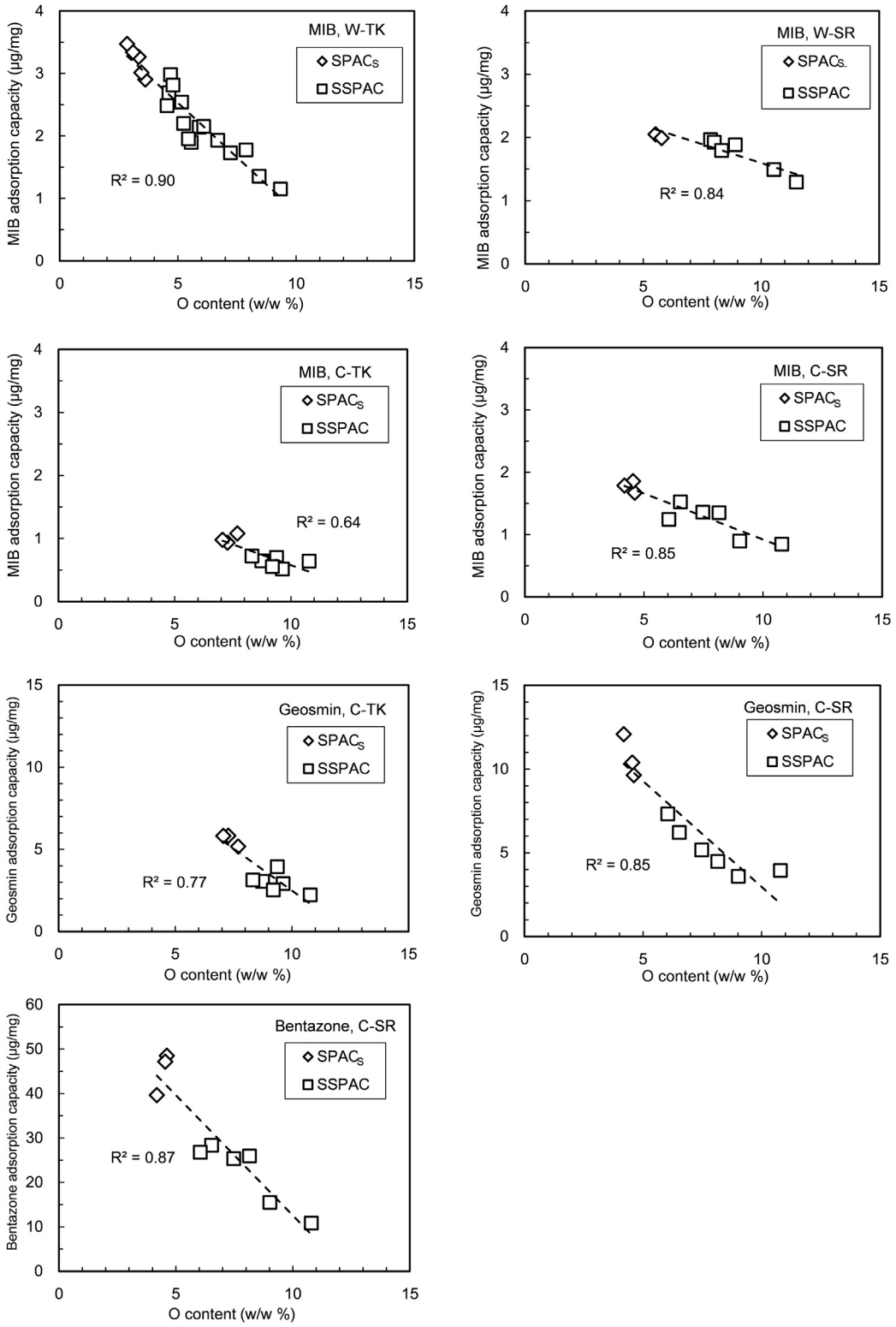

Fig. 2. Correlation between adsorption capacity and oxygen content. The values on the y-axis were quantified in terms of the solid-phase concentration for an equilibrium liquid-phase concentration of 50 ng/L for MIB and geosmin and 5 μg/L for bentazone (see also Figs. 1S–4S).

amounts of basic groups may have cancelled out any observable change in the absorbance around 1700 cm^{-1}, particularly if basic groups were converted to acidic groups.

Thus, the results of the three analyses (elemental, Boehm titration, and FTIR) were in agreement, indicating that the micro-milling produced oxygen/hydrogen-containing acidic functional groups, including phenolic hydroxyl and carboxylic functional groups. The extent of the acidic group increase was twice that of the basic group decrease, and thus the formation of acidic groups could not have been entirely due to the conversion of basic groups to

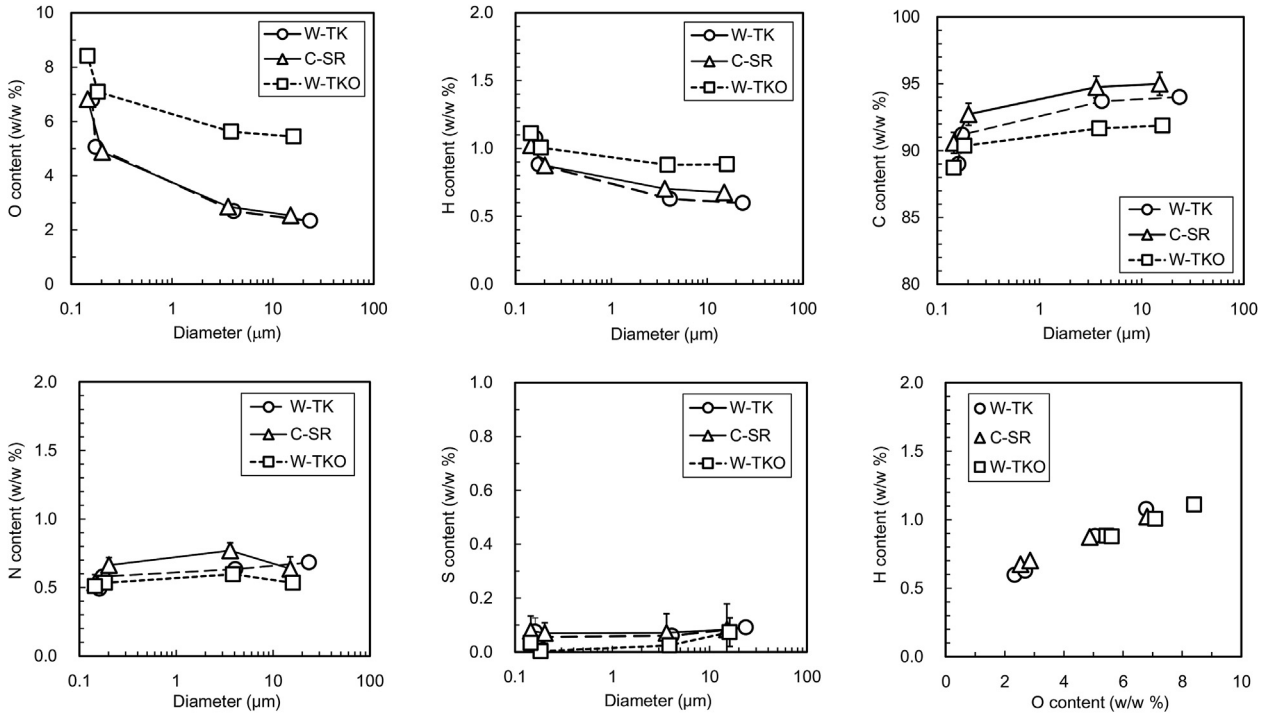

Fig. 3. Changes of O, H, C, N, and S content versus AC particle diameter during milling. The lower right panel is a plot of the relationship between the O and H content.

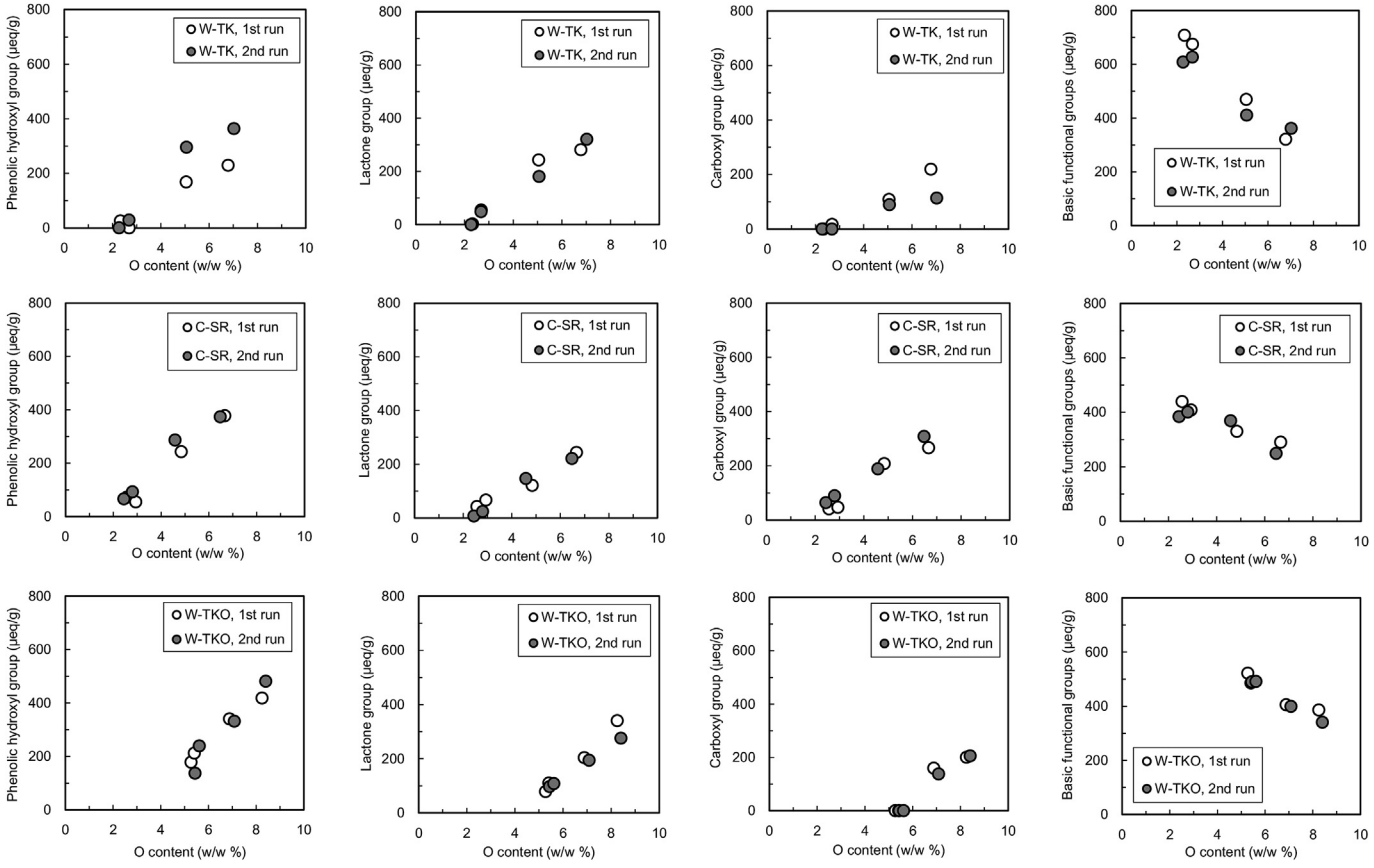

Fig. 4. Change in the amount of phenolic hydroxyl, lactone, carboxyl, and basic functional groups versus oxygen content during milling. Upper panels are for W-TK AC; middle panels are for C-SR; lower panels are for W-TKO.

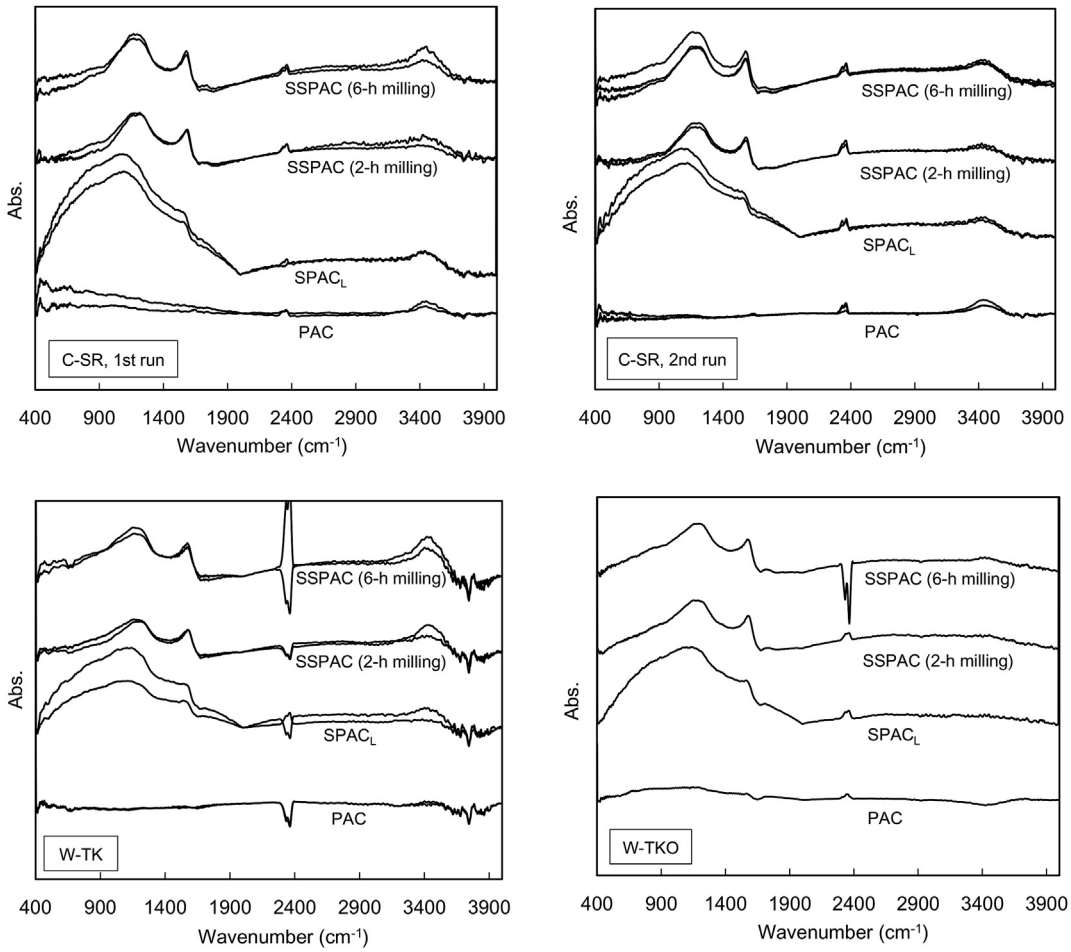

Fig. 5. FTIR spectra of the ACs. Upper panels are for the 1st and 2nd milling runs of C-SR AC; lower left panel is for W-TK; lower right panel is for W-TKO.

acidic groups. New surfaces generated by the fracture of particles during milling exhibit high chemical reactivity due to unsaturated carbon atoms at the graphene edge, which are crystallographically disordered and can be functionalized by oxygen or hydrogen. Welham and Williams (1998) ball-milled graphite and AC in a vacuum for up to 1000 h and reported that the ignition temperature of graphite decreased with increasing milling time and that this decrease was concomitant with a large increase in non-crystalline carbon. Thus, the formation of oxygen/hydrogen-containing groups is likely related to increased reactivity due to a reduction in crystallinity at the particle surface.

Finally, the hypothesis that the reduction of adsorption capacity by micro-milling is due to the formation of oxygen-containing functional groups was verified. These functional groups were acidic oxygen/hydrogen-containing functional groups including carboxylic, phenolic hydroxyl and lactone groups. This conclusion is in consistency with the previous researches for chemical and thermal-treated ACs of conventional-size powdered and granular forms which report that MIB adsorptions were impacted by total surface acidity (Chestnutt et al., 2007; Tennant and Mazyck, 2007).

3.3. Factors affecting the production of oxygen/hydrogen-containing functional groups

3.3.1. Contribution of DO

To investigate the cause of the oxygen/hydrogen content increase, we operated the mill under several operation conditions. Pan et al. (2017a) reported that AC oxidation was partially attenuated when the oxygen in the water and adsorbed on the AC were removed before milling, the introduction of oxygen during milling was prevented, and the rotational speed in the milling was lowered from 12 to 8 m/s.

In our study, we measured DO concentration during milling (Fig. 6). At a milling speed of 8 m/s, DO concentration decreased slowly and was reduced by half at 240 min of milling. However, at

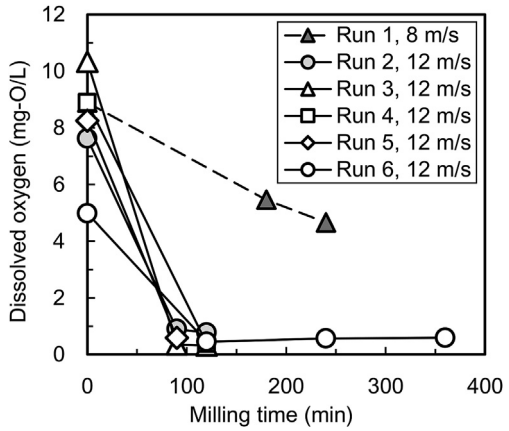

Fig. 6. Change of DO concentration during milling of W-TK AC.

the higher milling speed of 12 m/s, we observed a dramatic decrease of DO; by 100 min after the start of milling, DO was <1 mg/L. Although the DO concentration dropped, we found that the oxygen content of the ACs gradually increased with increasing milling time, even after 100 min (Fig. 7). No change of DO concentration was observed without AC slurry (data not shown).

We then converted the oxygen content (mass of oxygen per mass of AC) to mass of oxygen per liter of AC slurry because the grinding was conducted at a fixed AC mass concentration (Fig. 7). Before grinding, the oxygen mass per liter of AC slurry was around 300 mg-O/L. However, under high-speed milling (12 m/s) it had increased to around 700 mg-O/L at 120 min, and under low-speed milling (8 m/s) it had increased to around 500 mg-O/L at 180 min. These changes in mass of oxygen per liter of AC slurry (200 and 400 mg-O/L for low- and high-speed milling, respectively) were very large compared with the change of DO. Any reaction that increases the oxygen content of AC and promotes the formation of oxygen-containing functional groups could have accompanied the consumption of DO in the slurry, but the extent of the DO decrease in the slurry did not quantitatively explain the increase in oxygen content. However, the possibility remained that DO introduced from the air to the slurry may have caused the increase of oxygen content in the ACs.

To confirm the contribution of DO to the oxygen content increase, we milled AC particles under anoxic conditions and then determined the elemental composition of the AC particles. Fig. 7 (closed plots) shows the change of oxygen content of the ACs during anoxic milling. The change of oxygen content with time during anoxic milling was smaller than that observed during normal milling. Thus, the DO in AC slurry does affect the oxygen increase in AC particles, but the effect is limited. The increase of oxygen content in the AC particles was influenced by milling speed, even under anoxic conditions, again indicating that the DO was not strongly related to the oxygen content increase in AC particles. These results verified that DO was not a major cause of the oxygen content increase.

3.3.2. Oxidant formation during milling

Water containing reducing substances (SO_3^- and NO_2^- ions) were introduced into the milling chamber, and then the mill was operated (details are described in SI). There were no or insignificant change in the concentrations (Figs. 7S and 8S). In reference to the generation of gaseous hydrogen during the mechanochemical treatment of metal oxides in water (Domen et al., 2000; Hara et al., 2000; Kazunari et al., 2000), we tried to collect gas present above the water; however, no gas was collected, and so we concluded that no gas was generated.

Next, the possibility of the formation of an oxidant, hydroxyl radical, during milling was investigated by using two probe compounds: 1,4-dioxane and salicylic acid (details are described in SI). 1,4-Dioxane is decomposed by hydroxyl radical but not by oxygen, ozone, or chlorine (Adams et al., 1994; Coleman et al., 2007; Hill et al., 1997; Klečka and Gonsior, 1986; Matsushita et al., 2015; Suh and Mohseni, 2004). During milling, however, 1,4-dioxane concentration did not change (Fig. 9S). Salicylic acid is also decomposed by hydroxyl radical (Jen et al., 1998; Karnik et al., 2007; Quan et al., 2007; Tabatabaei and Abbott, 1999) to 2,3-dihydroxybenzoic acid (2,3-DHBA) and 2,5-dihydroxybenzoic acid (2,5-DHBA) (Fig. 10S). During operation of the micro-mill, we observed a decrease of salicylic acid concentration (Fig. 11S), but the formation of 2,3-DHBA and 2,5-DHBA was not observed (Fig. 12S). Thus, we concluded that hydroxyl radicals were not formed during milling. The decrease in salicylic acid would be caused by any mechanochemical reaction, but no specific mechanism was identified.

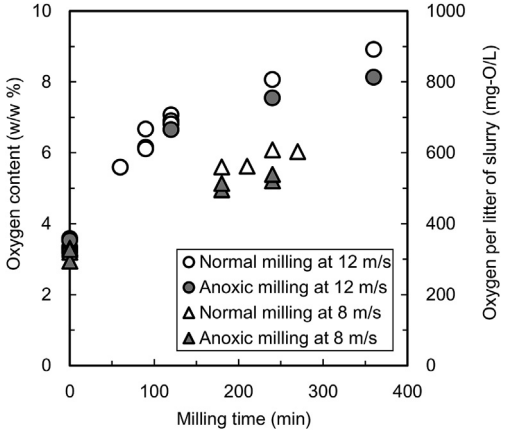

Fig. 7. Change of oxygen content of AC during milling. W-TK AC (10 g/L) was used; therefore, 10% oxygen content was converted to 1000 mg oxygen per liter of slurry.

3.3.3. Role of water in the formation of oxygen/hydrogen-containing functional groups

The results of the investigations described in the previous two sections suggested that a mechanochemical reaction that produced oxygen/hydrogen-containing functional groups in the ACs occurred during milling. Newly formed surfaces of milled AC exhibit extremely high chemical reactivity because of a lack of chemical bond saturation, resulting in surface re-formation by chemical reaction with the surrounding water (Balaz et al., 2013; Berndt, 2004).

Oxygen and hydrogen in the oxygen/hydrogen-containing functional groups formed on the AC particle surface during milling could have come from water molecules including hydroxide ions. To explore this possibility, we milled a $SPAC_L$ (W-TK) slurry containing water-^{18}O. Fig. 8 shows the change of $\delta^{18}O$ as the particle size decreased during anoxic milling. We observed a marked increase in the amount of $\delta^{18}O$ in SSPAC after milling in water-^{18}O compared with the amount in $SPAC_L$. In addition, the amount of $\delta^{18}O$ in SSPAC was higher when a longer milling time was used (6 h vs. 2 h). In contrast, $\delta^{18}O$ did not increase when the SSPAC was simply mixed with water-^{18}O for 2–6 h. These results clearly indicate that oxygen from the surrounding water was introduced into the AC when the AC particles were milled.

The diamonds in Fig. 8 are $\delta^{18}O$ values that were predicted by taking the mass balance of the oxygen content under the assumption that the additional oxygen atoms in the SSPAC after micro-milling originated entirely from the surrounding water and were characterized by an $^{18}O/^{16}O$ ratio identical to that of the surrounding water. The observed $\delta^{18}O$ values were lower than the predicted values. We assume this discrepancy was due to exchange of ^{18}O with ^{16}O during sample capsulation, transportation, and storage before isotope analysis. This was inferred from the following two results. First, the $\delta^{18}O$ values were higher when the AC samples were capsuled under anoxic conditions in a glovebox filled with nitrogen gas. Second, the $\delta^{18}O$ values were lower with longer elapsed time between sample production and analysis (Fig. 15S). The isotope analysis shown in Fig. 8 was conducted 5 days after the SSPAC samples were produced; 5 days was the minimum interval for sample transportation. There is also the possibility of a kinetic isotope effect in which water-^{18}O exhibited lower rate of reaction than water-^{16}O, so the $^{18}O/^{16}O$ ratio of the oxygen-containing groups formed by the reaction would be lower than that of the water (Fry, 2007).

Overall, the data indicate that oxygen/hydrogen-containing functional groups in the AC came from the water used to make the AC slurry. Specifically, hydroxide ions formed by the

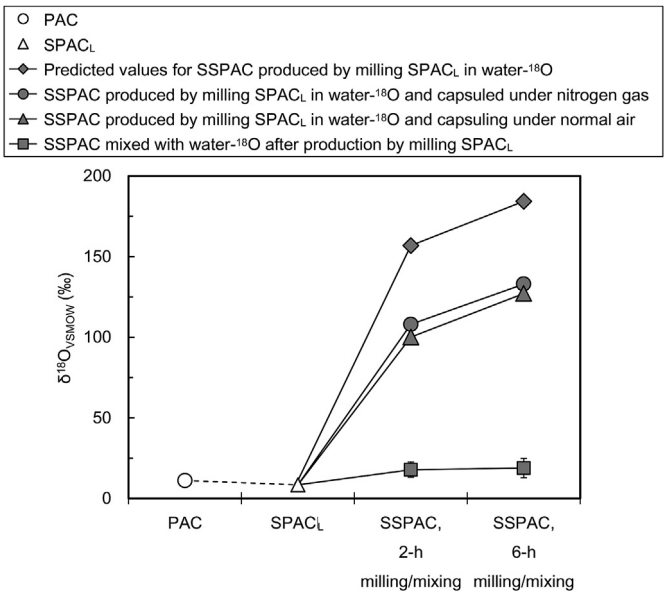

Fig. 8. Isotope ratio for oxygen-18 (^{18}O) and oxygen-16 (^{16}O). Predicted values (closed diamond plots) were obtained by taking the mass balance of the oxygen content under the assumption that the additional oxygen atoms in the SSPAC after milling originated entirely from the surrounding water and were characterized by an $^{18}O/^{16}O$ ratio identical to that of the surrounding water. Control values (closed rectangular plots) were obtained by stirring SSPAC water-^{18}O. The carbon was W-TK.

dissociation of water likely reacted with the newly formed surfaces of milled AC to form oxygen/hydrogen-containing functional groups. This conclusion is further supported by the decrease of the pH of the AC slurry with increasing oxygen content during milling (Fig. 16S).

4. Conclusions

1) Adsorption capacities of MIB, geosmin, and bentazone increased with decreasing particle diameter in the micron size range, but decreased with decreasing particle diameter in the submicron size range. The reduction of adsorption capacity by micro-milling was due to a decrease of hydrophobicity at the AC particle surface due to the formation of acidic functional groups containing oxygen and hydrogen.
2) With increasing duration of micro-milling, the amount of acidic functional groups, as determined by Boehm method, as well as the oxygen and hydrogen content, as determined by elemental analysis, in the AC particles was increased. The acidic functional groups included carboxylic, phenolic hydroxyl and lactone groups. With increased duration of micro-milling, the total (acidic and basic) number of functional groups increased, whereas the amount of basic functional groups decreased. With increased duration of milling, increases in FTIR peaks at 1200, 1580, and 3400 cm^{-1} were observed. These peaks were assigned to carboxylic and phenolic hydroxyl functional groups.
3) The increase of oxygen content in AC particles during milling was somewhat attenuated under anoxic conditions. The DO concentration in the slurry decreased during milling at high-speed but not at low-speed. However, the decrease of oxygen content was much smaller than the increase of oxygen content in AC particles. Therefore, oxidation of the AC particles by DO played a minor role in the increase of oxygen content. No gas production was observed, nor was there any evidence of oxidant formation.
4) When AC was milled in water-^{18}O, the ^{18}O content of the AC increased. The pH of AC slurry decreased during micro-milling. Therefore, the oxygen in the oxygen/hydrogen-containing functional groups originated from the surrounding water, probably hydroxide ion. The new oxygen/hydrogen-containing functional groups in the AC likely arose from a mechanochemical reaction that occurred during the milling process. Newly formed surfaces of milled AC exhibit extremely high chemical reactivity because of the chemical bond unsaturation and therefore underwent surface re-formation by chemical reaction with hydroxide ion in the surrounding water and the formation of oxygen/hydrogen-containing functional groups.

Declaration of interests

The authors declare that they have no known competing financial interests or personal relationships that could have appeared to influence the work reported in this paper.

The authors declare the following financial interests/personal relationships which may be considered as potential competing interests:

Acknowledgments

This work was supported by JSPS KAKENHI Grant Number JP16H06362. The authors gratefully acknowledge Futamura Chemical and Osaka Gas Chemicals for providing PAC samples.

Appendix A. Supplementary data

Supplementary data to this article can be found online at https://doi.org/10.1016/j.watres.2019.02.019.

References

Adams, C.D., Scanlan, P.A., Secrist, N.D., 1994. Oxidation and biodegradability enhancement of 1,4-dioxane using hydrogen peroxide and ozone. Environ. Sci. Technol. 28 (11), 1812–1818.
Amaral, P., Partlan, E., Li, M., Lapolli, F., Mefford, O.T., Karanfil, T., Ladner, D.A., 2016. Superfine powdered activated carbon (S-PAC) coatings on microfiltration membranes: effects of milling time on contaminant removal and flux. Water Res. 100, 429–438.
Ando, N., Matsui, Y., Kurotobi, R., Nakano, Y., Matsushita, T., Ohno, K., 2010. Comparison of natural organic matter adsorption capacities of super-powdered activated carbon and powdered activated Carbon. Water Res. 44 (14), 4127–4136.
Balaz, P., Achimovicova, M., Balaz, M., Billik, P., Cherkezova-Zheleva, Z., Criado, J.M., Delogu, F., Dutkova, E., Gaffet, E., Gotor, F.J., Kumar, R., Mitov, I., Rojac, T., Senna, M., Streletskii, A., Wieczorek-Ciurowa, K., 2013. Hallmarks of mechanochemistry: from nanoparticles to technology. Chem. Soc. Rev. 42 (18), 7571–7637.
Barroso-Bogeat, A., Alexandre-Franco, M., Fernández-González, C., Gómez-Serrano, V., 2014. FT-IR analysis of pyrone and chromene structures in activated carbon. Energy Fuels 28 (6), 4096–4103.
Berndt, C.C., 2004. In: Davis, J.R. (Ed.), Handbook of Thermal Spray Technology. ASM International, pp. 147–158.
Biniak, S., Szymański, G., Siedlewski, J., Światkowski, A., 1997. The characterization of activated carbons with oxygen and nitrogen surface groups. Carbon 35 (12), 1799–1810.
Boehm, H.P., 1966. In: Eley, D.D., Pines, H., Weisz, P.B. (Eds.), Advances in Catalysis, vol. 16. Academic Press, New York, p. 179.
Boehm, H.P., 2002. Surface oxides on carbon and their analysis: a critical assessment. Carbon 40 (2), 145–149.
Bonvin, F., Jost, L., Randin, L., Bonvin, E., Kohn, T., 2016. Super-fine powdered activated carbon (SPAC) for efficient removal of micropollutants from wastewater treatment plant effluent. Water Res. 90, 90–99.
Chestnutt Jr., T.E., Bach, M.T., Mazyck, D.W., 2007. Improvement of thermal reactivation of activated carbon for the removal of 2-methylisoborneol. Water Res. 41 (1), 79–86.
Coleman, H.M., Vimonses, V., Leslie, G., Amal, R., 2007. Degradation of 1,4-dioxane in water using TiO2 based photocatalytic and H2O2/UV processes. J. Hazard Mater. 146 (3), 496–501.
Considine, R., Denoyel, R., Pendleton, P., Schumann, R., Wong, S.-H., 2001. The

influence of surface chemistry on activated carbon adsorption of 2-methylisoborneol from aqueous solution. Colloid. Surf. Physicochem. Eng. Asp. 179 (2–3), 271–280.
Domen, K., Ikeda, S., Takata, T., Tanaka, A., Hara, M., Kondo, J.N., 2000. Mechano-catalytic overall water-splitting into hydrogen and oxygen on some metal oxides. Appl. Energy 67 (1), 159–179.
Dunn, S.E., Knappe, D.R.U., 2013. DBP Precursor and Micropollutant Removal by Powdered Activated Carbon. Water Research Foundation, Denver, CO, USA.
Ellerie, J.R., Apul, O.G., Karanfil, T., Ladner, D.A., 2013. Comparing graphene, carbon nanotubes, and superfine powdered activated carbon as adsorptive coating materials for microfiltration membranes. J. Hazard Mater. 261 (0), 91–98.
Fanning, P.E., Vannice, M.A., 1993. A DRIFTS study of the formation of surface groups on carbon by oxidation. Carbon 31 (5), 721–730.
Fry, B., 2007. Stable Isotope Ecology. Springer, New York.
Fuente, E., Menéndez, J.A., Díez, M.A., Suárez, D., Montes-Morán, M.A., 2003. Infrared spectroscopy of carbon Materials: a quantum chemical study of model compounds. J. Phys. Chem. B 107 (26), 6350–6359.
Hara, M., Komoda, M., Hasei, H., Yashima, M., Ikeda, S., Takata, T., Kondo, J.N., Domen, K., 2000. A study of mechano-catalysts for overall water splitting. J. Phys. Chem. B 104 (4), 780–785.
Heijman, S.G.J., Hamad, J.Z., Kennedy, M.D., Schippers, J., Amy, G., 2009. Submicron powdered activated carbon used as a pre-coat in ceramic micro-filtration. Desalination and Water Treatment 9 (1–3), 86–91.
Hill, R.R., Jeffs, G.E., Roberts, D.R., 1997. Photocatalytic degradation of 1,4-dioxane in aqueous solution. J. Photochem. Photobiol. Chem. 108 (1), 55–58.
Jen, J.-F., Leu, M.-F., Yang, T.C., 1998. Determination of hydroxyl radicals in an advanced oxidation process with salicylic acid trapping and liquid chromatography. J. Chromatogr. A 796 (2), 283–288.
Jiang, W., Xiao, F., Wang, D.S., Wang, Z.C., Cai, Y.H., 2015. Removal of emerging contaminants by pre-mixed PACl and carbonaceous materials. RSC Adv. 5 (45), 35461–35468.
Kanaya, S., Kawase, Y., Mima, S., 2015. Drinking Water Treatment Using Superfine PAC (SPAC): Design and Successful Operation History in Full-Scale Plant. American Water Works Association, Salt Lake City, Utah, USA, pp. 624–631.
Karnik, B.S., Davies, S.H., Baumann, M.J., Masten, S.J., 2007. Use of salicylic acid as a model compound to investigate hydroxyl radical reaction in an ozonation–membrane filtration hybrid process. Environ. Eng. Sci. 24 (6), 852–860.
Kazunari, D., Kondo, Junko N., Michikazu, H., Tsuyoshi, T., 2000. Photo- and mechano-catalytic overall water splitting reactions to form hydrogen and oxygen on heterogeneous catalysts. Bull. Chem. Soc. Jpn. 73 (6), 1307–1331.
Klečka, G.M., Gonsior, S.J., 1986. Removal of 1,4-dioxane from wastewater. J. Hazard Mater. 13 (2), 161–168.
Matsui, Y., Fukuda, Y., Murase, R., Aoki, N., Mima, S., Inoue, T., Matsushita, T., 2004. Micro-ground powdered activated carbon for effective removal of natural organic matter during water treatment. Water Sci. Technol. Water Supply 4 (4), 155–163.
Matsui, Y., Nakao, S., Sakamoto, A., Taniguchi, T., Pan, L., Matsushita, T., Shirasaki, N., 2015. Adsorption capacities of activated carbons for geosmin and 2-methylisoborneol vary with activated carbon particle size: effects of adsorbent and adsorbate characteristics. Water Res. 85, 95–102.
Matsui, Y., Nakao, S., Taniguchi, T., Matsushita, T., 2013. Geosmin and 2-methylisoborneol removal using superfine powdered activated carbon: shell adsorption and branched-pore kinetic model analysis and optimal particle size. Water Res. 47 (8), 2873–2880.
Matsui, Y., Yoshida, T., Nakao, S., Knappe, D.R.U., Matsushita, T., 2012. Characteristics of competitive adsorption between 2-methylisoborneol and natural organic matter on superfine and conventionally sized powdered activated carbons. Water Res. 46 (15), 4741–4749.
Matsushita, T., Hirai, S., Ishikawa, T., Matsui, Y., Shirasaki, N., 2015. Decomposition of 1,4-dioxane by vacuum ultraviolet irradiation: study of economic feasibility and by-product formation. Process Saf. Environ. Protect. 94, 528–541.
Noh, J.S., Schwarz, J.A., 1990. Effect of HNO3 treatment on the surface acidity of activated carbons. Carbon 28 (5), 675–682.
Pan, L., Matsui, Y., Matsushita, T., Shirasaki, N., 2016. Superiority of wet-milled over dry-milled superfine powdered activated carbon for adsorptive 2-methylisoborneol removal. Water Res. 102, 516–523.
Pan, L., Nishimura, Y., Takaesu, H., Matsui, Y., Matsushita, T., Shirasaki, N., 2017a. Effects of decreasing activated carbon particle diameter from 30 μm to 140 nm on equilibrium adsorption capacity. Water Res. 124, 425–434.
Pan, L., Takagi, Y., Matsui, Y., Matsushita, T., Shirasaki, N., 2017b. Micro-milling of spent granular activated carbon for its possible reuse as an adsorbent: remaining capacity and characteristics. Water Res. 114, 50–58.
Partlan, E., Davis, K., Ren, Y., Apul, O.G., Mefford, O.T., Karanfil, T., Ladner, D.A., 2016. Effect of bead milling on chemical and physical characteristics of activated carbons pulverized to superfine sizes. Water Res. 89, 161–170.
Pendleton, P., Wong, S.H., Schumann, R., Levay, G., Denoyel, R., Rouquero, J., 1997. Properties of activated carbon controlling 2-Methylisoborneol adsorption. Carbon 35 (8), 1141–1149.
Pendleton, P., Wu, S.H., Badalyan, A., 2002. Activated carbon oxygen content influence on water and surfactant adsorption. J. Colloid Interface Sci. 246 (2), 235–240.
Quan, X., Zhang, Y., Chen, S., Zhao, Y., Yang, F., 2007. Generation of hydroxyl radical in aqueous solution by microwave energy using activated carbon as catalyst and its potential in removal of persistent organic substances. J. Mol. Catal. Chem. 263 (1), 216–222.
Quinlivan, P.A., Li, L., Knappe, D.R., 2005. Effects of activated carbon characteristics on the simultaneous adsorption of aqueous organic micropollutants and natural organic matter. Water Res. 39 (8), 1663–1673.
Shafeeyan, M.S., Daud, W.M.A.W., Houshmand, A., Shamiri, A., 2010. A review on surface modification of activated carbon for carbon dioxide adsorption. J. Anal. Appl. Pyrol. 89 (2), 143–151.
Suh, J.H., Mohseni, M., 2004. A study on the relationship between biodegradability enhancement and oxidation of 1,4-dioxane using ozone and hydrogen peroxide. Water Res. 38 (10), 2596–2604.
Tabatabaei, A.R., Abbott, F.S., 1999. LC/MS analysis of hydroxylation products of salicylate as an indicator of in vivo oxidative stress. Free Radic. Biol. Med. 26 (7), 1054–1058.
Tennant, M.F., Mazyck, D.W., 2007. The role of surface acidity and pore size distribution in the adsorption of 2-methylisoborneol via powdered activated carbon. Carbon 45 (4), 858–864.
Welham, N.J., Williams, J.S., 1998. Extended milling of graphite and activated carbon. Carbon 36 (9), 1309–1315.
WHO, 2011. Guidelines for Drinking-Water Quality. World Health Organization, Geneva, Switzerland.